

Designing power efficient transistors using narrow bandwidth materials from the MA_2Z_4 monolayer series

Keshari Nandan,^{1,*} Somnath Bhowmick,^{2,†} Yogesh S. Chauhan,^{1,‡} and Amit Agarwal^{3,§}

¹*Department of Electrical Engineering, Indian Institute of Technology Kanpur, India, 208016.*

²*Department of Materials Science and Engineering,
Indian Institute of Technology Kanpur, India, 208016.*

³*Department of Physics, Indian Institute of Technology Kanpur, India, 208016.*

(Dated: November 18, 2022)

The subthreshold leakage current in transistors has become a critical limiting factor for realizing ultra-low-power transistors. The leakage current is predominantly dictated by the long thermal tail of the charge carriers. We propose a solution to this problem by using narrow bandwidth semiconductors for limiting the thermionic leakage current by filtering out the high energy carriers. We specifically demonstrate this solution in transistors with laterally confined monolayer MoSi_2N_4 with different passivation serving as channel material. Remarkably, we find that the proposed narrow bandwidth devices can achieve a large ON/OFF current ratio with an ultra-low-power supply voltage of ~ 0.1 V, even for devices with ~ 5 nm gate length. We also show that several other materials share the unique electronic properties of narrow bandwidth conduction and valance bands in the same series.

I. INTRODUCTION

The main bottleneck in the design of ultra low-power transistors is the rate change of the ON current with the applied gate voltage¹. This is technically described as the lowering of the subthreshold slope (SS), which is a crucial figure of merit determining a transistor's performance. The SS is the smallest change in gate voltage, V_{GS} required to change the drain current, I_{DS} by one order of magnitude. The dissipation of energy by thermally excited charge carriers is facilitated by a existence of electronic states at high energies, and it sets a natural limit on the subthreshold slope to be $SS < 60$ mV/decade. This is known as the thermionic limit and this thermodynamic dissipation problem is referred to as Boltzmann's tyranny (see Fig. 1). Overcoming the Boltzmann tyranny by making $SS < 60$ mV/decade is currently one of the biggest challenges in conceptualizing ultra-low-power transistors.

Different strategies are being used to solve this problem. One strategy is to shorten the thermal tail, with tunnel field-effect transistors (FETs)²⁻⁴ being the most common device. Another strategy is to increase the barrier height's steepness with gate voltages, with Landau's FETs⁵⁻⁷ being the most common device. However, the tunneling transport limits the ON-state current to very low values in tunnel FETs, and there are several challenges in Landau FETs at both material and device levels. In fact, low hysteresis with the required ON-state current has not been achieved experimentally⁸⁻¹¹ in Landau FETs. In recent years, the rise of layered materials¹²⁻²⁹ has offered more opportunities to conceptualize and design energy-efficient logic devices³⁰⁻³³. For subthermionic switching, the Dirac cone in the electronic band structures of layered materials like graphene has also been used to shorten the thermal tail^{34,35}.

Here, we present a solution to the problem of Boltzmann's tyranny, by using narrow bandwidth semiconductors as channel material. The narrow bandwidth

of the conduction/valance band naturally restricts the long thermal tail of the charge carriers, reduces the thermionic current in the OFF state [see Figure 1 (f)], and solves the problem of Boltzmann's tyranny. We demonstrate that using this solution, the devices can achieve a large ON/OFF current ratio with an ultra-low-power supply voltage of ~ 0.1 V, down to ~ 5 nm gate length. While the concept is very general, we demonstrate this in the laterally confined monolayer of the recently synthesized MoSi_2N_4 monolayers³⁶. Monolayer MoSi_2N_4 is an excellent semiconductor with outstanding physical, mechanical, thermal, electronic, and metal contact properties, which are at par with most other 2-D semiconductors³⁶⁻⁴². We assess the transistor performance of differently passivated monolayers of MoSi_2N_4 , by using first principles-based nanoscale device simulations. All single and dual-gate devices show ultra-low-power steep slope transistor characteristics down to short channel lengths. Additionally, we show that other members of the MoSi_2N_4 family also show these unique electronic properties in their laterally confined structures. This opens up new avenues for exploring 2-D transistors for ultra-power-efficient computing.

This paper is organized as follows: In Sec. II A, we describe the origin of low power dissipation and subthermionic switching in transistors with narrow bandwidth source materials. As an example of this, we discuss the electronic properties of passivated MoSi_2N_4 nanoribbons, which host narrow bandwidth conduction band in Sec. II B. In Sec. II C, we describe the electrical properties of transistors made from these structures. In Secs. II D and II E, we show that several differently terminated MoSi_2N_4 , and other materials in the MoSi_2N_4 series also host narrow conduction or valance bands. These can also serve as power efficient source or channel materials. Finally, we summarize our findings in Sec. III.

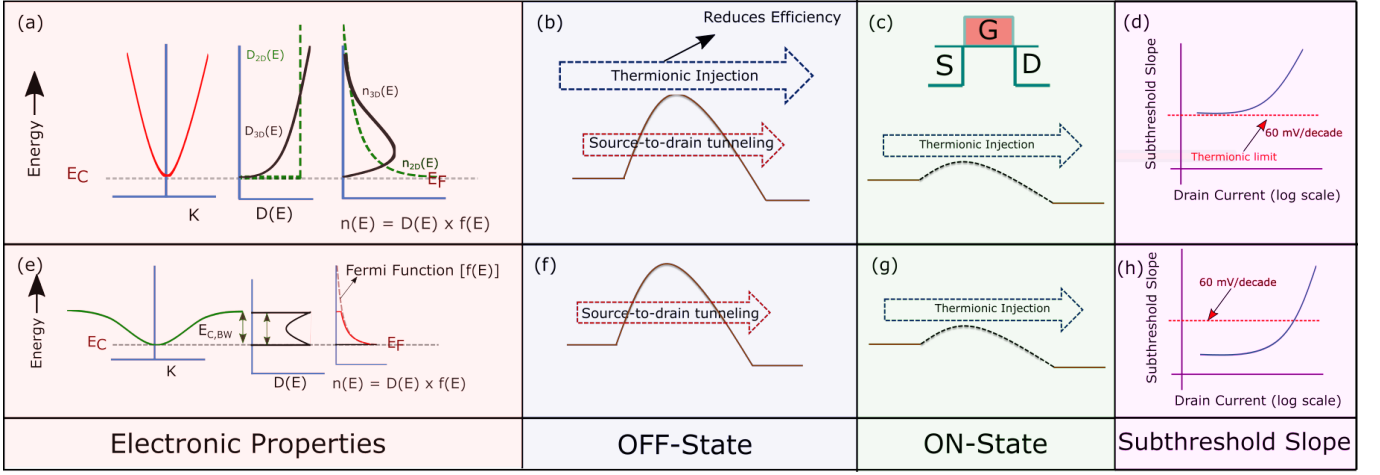


Figure 1. Schematic depicting the idea of ultra-low-power transistors based on narrow bandwidth materials, which suppress the thermionic injection in the OFF state. (a) The energy dispersion, the density of states $[D(E)]$, and electron density $[n(E)]$ with a long thermal tail in conventional 3D and 2D materials. (b) The OFF state has an unwanted leakage current arising from the long thermal tail of the carriers (thermionic injection) and tunneling. (c) The ON state with a lowered potential barrier and the ON current arising from the thermionic injection. (d) The subthreshold slope is limited to 60 mV/decade in conventional transistors of 3-D and 2-D semiconductors due to the long thermal tail. (e) Novel semiconductors with narrow bandwidth, which suppresses the thermal tail of the carriers. (f) The lack of a long thermal tail of carriers suppresses the thermionic injection in the OFF state. This enables subthermionic switching leading to ultra-efficient transistors. (g) The ON state. (h) The subthreshold slope overcomes the thermionic limit due to the short thermal tail in these narrow bandwidth semiconductors.

II. RESULTS AND DISCUSSIONS

A. Narrow bandwidth enabled subthermionic switching

Here, we highlight the idea of reduced power dissipation or subthermionic switching in transistors by using low bandwidth materials. The SS is defined as

$$SS \equiv \frac{\partial V_{GS}}{\partial \log_{10} I_{DS}} = \underbrace{\frac{\partial V_{GS}}{\partial \phi_b}}_m \times \underbrace{\frac{\partial \phi_b}{\partial \log_{10} I_{DS}}}_n. \quad (1)$$

Here, ϕ_b is the barrier height from source-to-channel, and the first and second terms in Eq. (1) are the body factor (m) and the transport factor (n), respectively. To connect this to the electronic bandwidth, we note that the electron density in a n-type 3-D semiconductor at a given energy is specified by the product of the density of states and the Fermi function: $n(E) = D(E) \times f(E)$. Here, $f(E) = 1/[1 + \exp(E/k_B T)]$ is the Fermi function. For 3-D systems, we have $D_{3D}(E) \propto \sqrt{E}$. As a result, the carrier density in conventional bulk semiconductors like Si/Ge decays sub-exponentially with E , with an infinitely long thermal tail (see Figure 1). Similarly, the electron density in 2-D semiconductors is given by $D_{2D}(E) \propto E^0$ and we have $n(E) \propto f(E)$. This implies that the carrier density in 2-D systems also decays exponentially with E , and it also has an infinitely long thermal tail. Therefore, during the onset of conduction in conventional transistors comprised of 3D or 2D channel material, the current is determined by the thermally activated carriers and we have $I_{DS} \sim \exp(-\phi_t/\phi_b)$, with $\phi_t \equiv k_B T/q$ being the

temperature scale. This yields, $n \cong \ln(10)\phi_t$. In conventional transistors, the electrostatic coupling between gate and channel dictates that $m > 1$. Thus, in conventional transistors, the SS is limited to a value of $SS > 60$ mV/decade at room temperature (300 K), imposing a stiff limitation on their performance. It is typically referred to as the Boltzmann tyranny.

One possible solution to the problem of Boltzmann's tyranny arising from the long thermal tail, is to have a narrow bandwidth conduction band separated from the higher conduction band by a large energy gap. This cuts off the thermal tail above the potential barrier in the channel and suppresses the thermionic injection at a low gate-to-source bias (V_{GS}) [see Figure 1]. In this scenario, direct source-to-drain tunneling (SDT)⁴³ will leak a small amount of current in the OFF state (I_{DS}), which strongly depends on the tunneling carrier's effective mass and width of the tunneling barrier (source-to-drain barrier). With the increase in V_{GS} , the potential barrier in the channel decreases, and the current conduction mechanism changes from SDT to thermionic, resulting in a sudden increase in the drain current. This enables n to have much smaller values and consequently we can have $SS < 60$ mV/decade, opening up possibilities for designing very power efficient transistors. This is the main idea, and highlight of this paper. In the rest of the paper, we demonstrate this idea of narrow band 2-D semiconductors overcoming Boltzmann's tyranny, using laterally confined MoSi_2N_4 as a channel material for realizing steep-slope and power-efficient logic electronic switches. To explicitly show this, we first establish the presence of a

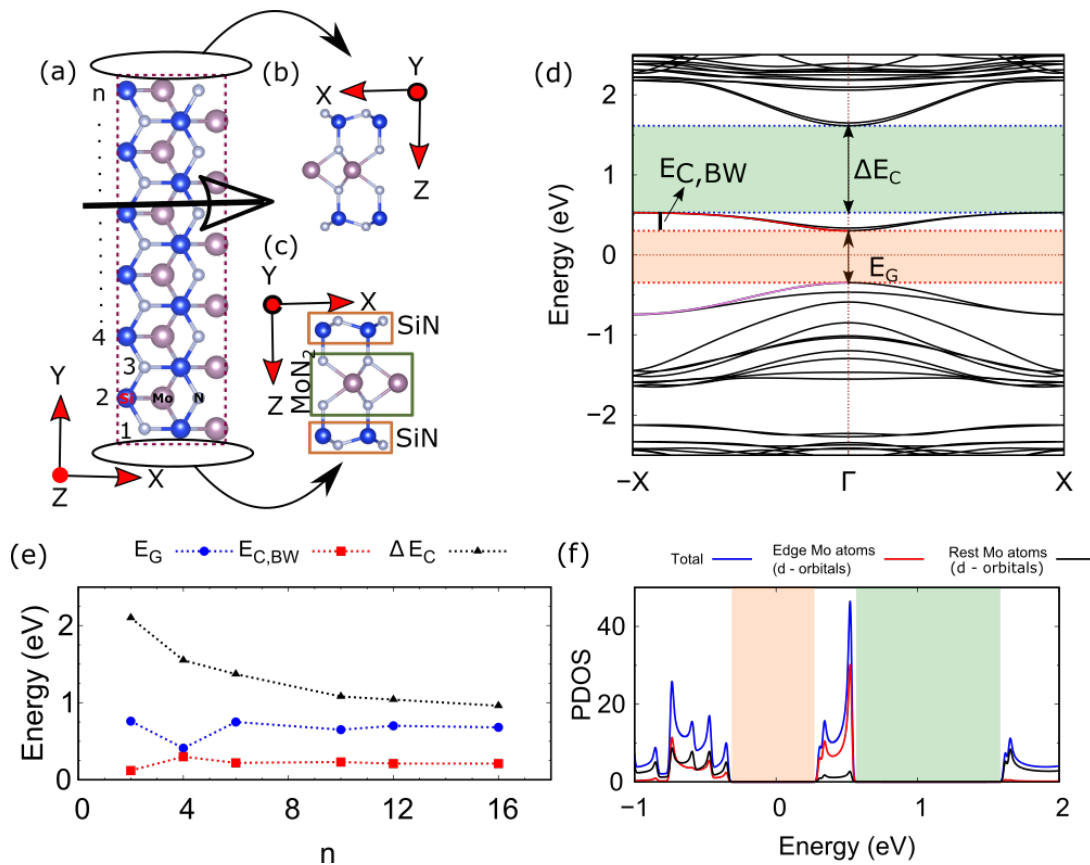


Figure 2. (a) Unit cell of a laterally confined (in the y -direction) monolayer of MoSi₂N₄. We refer to it as n -MoSi₂N₄, depending on the number (n) of bulk unit cells along the confinement direction. (b) and (c) show the zoomed view of the top and bottom edge of the structure, respectively. (d) The electronic bandstructure of H-terminated 10-MoSi₂N₄. (e) Variation of the bandgap (E_G), the bandwidth of the conduction band ($E_{C,BW}$), and the gap of the first conduction band from the higher conduction band (ΔE_C) with the width of the nanoribbon in the confinement direction. (f) The atom and orbital resolved density of states of the edge and inner Mo atoms. Clearly, the narrow conduction band states arise from the edge Mo atoms.

narrow bandwidth conduction band in laterally confined MoSi₂N₄ by calculating their electronic properties.

B. Electronic properties of H terminated MoSi₂N₄

We calculate the electronic properties of monolayer (2-D) MoSi₂N₄ for benchmarking our calculations [see Figure S1 and Table S1 in the Supporting Information (SI)⁴⁴]. The results are found to be consistent with those reported in the literature^{36,45}. We find the bandgap predicted by DFT with PBE functional ($E_G = 1.86$ eV) to be very close to the experimental value ($E_{G,exp} = 1.94$ eV)³⁶. Orbital projected density of states (PDOS) reveals that in the vicinity of the conduction band minima (0.1 eV around CBM) $\sim 82\%$ and $\sim 15\%$ of the total DOS are contributed by the d -orbitals of molybdenum (Mo) and p -orbitals of nitrogen (N), respectively. Our charge distribution and orbital projected density of states (PDOS) analysis reveal that Mo- d_{z^2} and N- p_z orbitals hybridize to form the σ -bonds. As a result, bonding and anti-bonding orbitals form VBM and CBM, respectively [see Figure S2 of SI⁴⁴ for further details].

Starting from the optimized structure of 2-D monolayer, we construct n -MoSi₂N₄ nanoribbons (periodic along the x -direction) by stacking ($n/2$) number of unit cells along the y -direction [see Figure 2]. After creating the nanoribbon (say 10-MoSi₂N₄), the structure is relaxed once again before performing the electronic structure calculation. If dangling bonds of the edge atoms are left unpassivated, such a 10-MoSi₂N₄ nanoribbon is a semiconductor with a bandgap of $E_G \sim 0.9$ eV [see Figure S3 of SI⁴⁴ and related discussion].

To eliminate the effect of the dangling bonds, we use hydrogen (H) atoms to terminate the edges. Hydrogen is commonly used for edge termination in experiments^{46–48}, as the process can be easily controlled by the pressure and temperature of the H₂ gas. To keep the coordination number unchanged, each of the edge Mo, N, and Si atoms is terminated by two H atoms, one H atom, and one H atom, respectively. The electronic band structure of the optimized structure is shown in Figure 2 (d), along the high symmetry path ($-X - \Gamma - X$). The two lowest energy conduction bands have narrow bandwidth ($E_{C,BW}$), and they are separated from nearby bands by

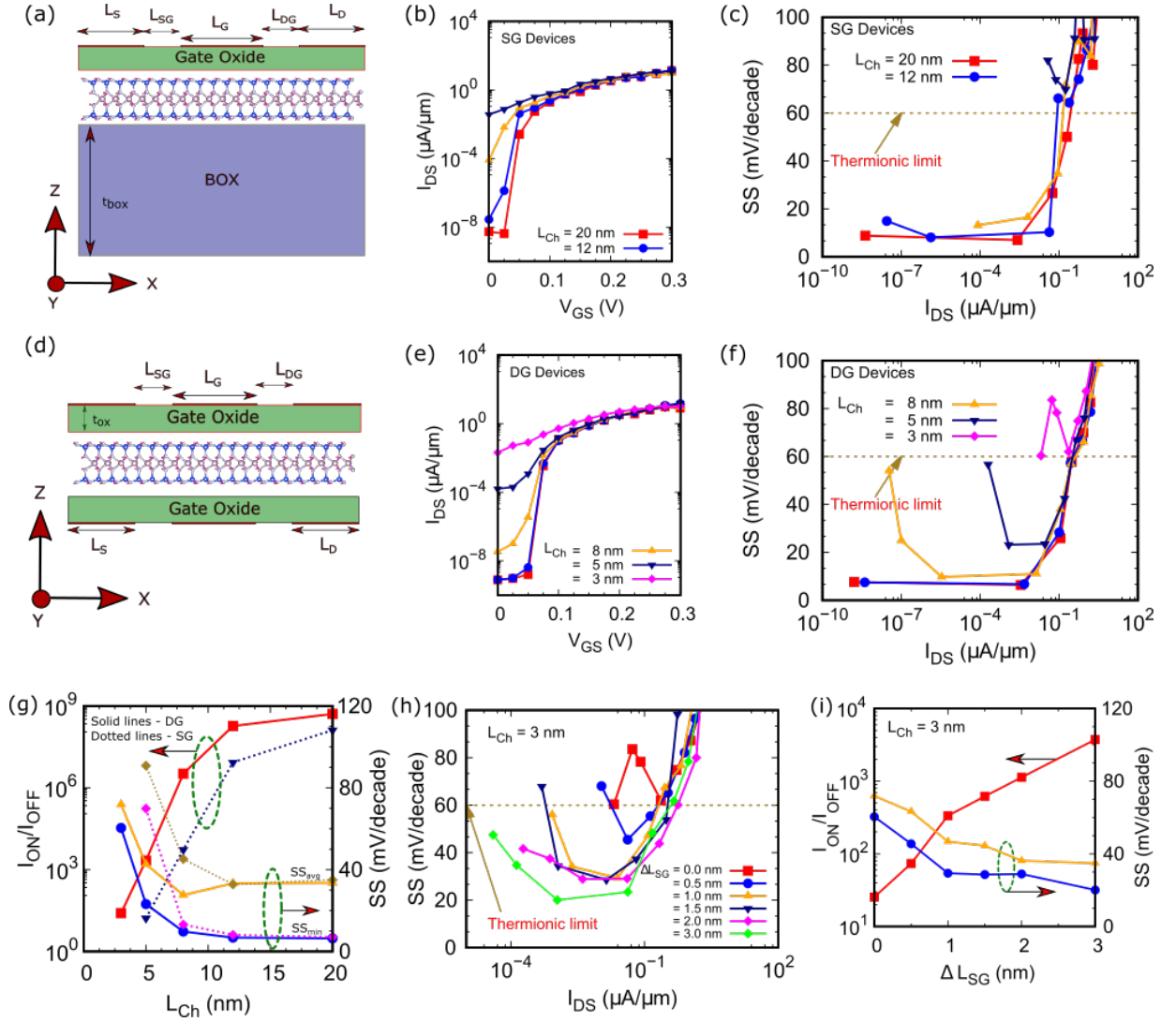


Figure 3. Schematic of a (a) single-gate (SG) device with SiO_2 as the BOX and gate oxide with thickness t_{box} and t_{ox} , respectively. (b) Transfer characteristics in semilogarithmic scale and (c) subthreshold slope vs drain current of SG devices for various channel lengths (L_{Ch}). Schematic of (d) a double-gate (DG) devices and its (e) transfer characteristics in semilogarithmic scale and (f) subthreshold slope vs drain current for various L_{Ch} . Both the SG and DG devices use H terminated 10-MoSi₂N₄ as the channel material. (g) $I_{\text{ON}}/I_{\text{OFF}}$ and SS vs L_{Ch} for SG and DG devices comprised of H terminated 10-MoSi₂N₄. (h) SS vs drain current and (i) $I_{\text{ON}}/I_{\text{OFF}}$ and SS vs ΔL_{SG} for DG device for a H terminated 10-MoSi₂N₄ with $L_{\text{Ch}} = 3$ nm. The devices with $SS < 60$ mV/decade indicate highly power efficient transistors.

a relatively large gap of ΔE_{C} . The variation of E_{G} , $E_{\text{C,BW}}$, and ΔE_{C} with n are plotted in Figure 2 (e) for H-terminated n -MoSi₂N₄. As n increases, E_{G} , $E_{\text{C,BW}}$, and ΔE_{C} saturate to ~ 0.7 eV, ~ 0.2 eV, and ~ 1.0 eV, respectively. These localized conduction bands, in H-terminated 10-MoSi₂N₄, are predominated by d -orbitals of edge Mo atoms, as shown in Figure 2 (f). See Figure S4 of SI⁴⁴ for more details. Such a unique combination of electronic states can potentially achieve the target of sub-60 mV/decade switching in transistors by cutting off the thermionic current in the OFF-state.

C. Transistors based on H-terminated MoSi₂N₄

To evaluate the the transport properties and sub-60 mV/decade switching, we perform first-principles-based nanoscale device simulation of single-gate (SG) and double-gate (DG) devices composed of H-terminated 10-MoSi₂N₄. The schematics of devices are shown in Figure 3 (a) and (d), in which the main geometrical parameters are the gate length (L_{G}), source/drain length ($L_{\text{S/D}}$), source/drain-to-gate length ($L_{\text{SG/DG}}$), and oxide thickness (t_{ox}). SiO_2 is used as both gate oxide [$t_{\text{ox}} = 0.60$ nm] and box oxide [$t_{\text{box}} = 10$ nm]. The source/drain is electrostatically doped using source/drain gate with $L_{\text{S/D}} = 9.80$ nm, and $L_{\text{SG/DG}} = 0.20$ nm. The power

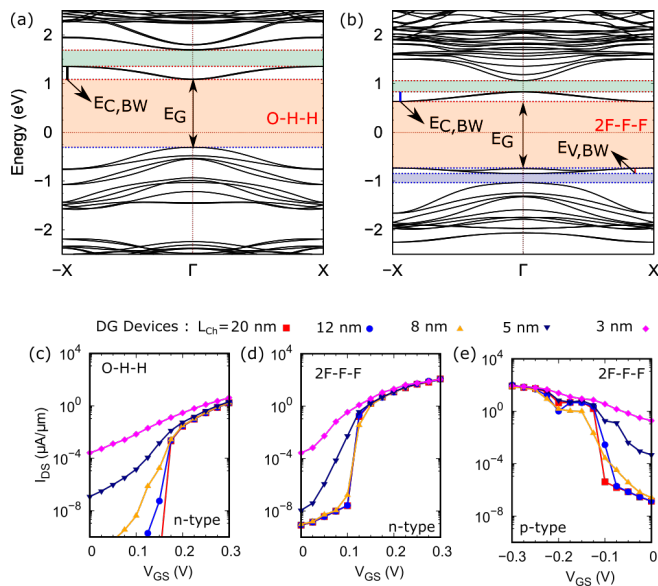


Figure 4. Narrow bandwidth electronic band structure of (a) O-H-H and (b) 2F-F-F terminated 10-MoSi₂N₄. In O-H-H terminated structure, the two lowest energy conduction bands have a narrow bandwidth. Interestingly, the two highest energy valance bands are also localized in energy with width $E_{V,BW}$ in addition to the bottom two energy localized conduction bands. The transport properties of DG devices include (c) O-H-H and (d, e) 2F-F-F as a channel material with $L_{Ch} = 20$ nm, 12 nm, 8 nm, 5 nm, and 3 nm.

supply voltage (V_{DD}) is 0.1 V. The devices' characteristics are shown by considering 200 parallelly connected chains of devices per μm along the z -direction³⁴.

The variation of the drain current with gate potential (transfer characteristics) and that of the SS with drain current for both SG and DG devices for various channel lengths L_{Ch} , are shown in Figure 3 (b, e) and (c, f), respectively. We find that over more than three decades of drain current in SG devices, the drain current exhibits subthermionic nature, with an average subthreshold slope of less than 46 mV/decade for $L_{Ch} \leq 8$ nm. They also show a good ON-OFF current ratio ($> 10^3$) with the minimum point subthreshold slope less than 25 mV/decade down to 8 nm channel length. The performance parameters of DG devices with $L_{Ch} \leq 5$ nm are the same as those of SG devices with $L_{Ch} \leq 8$ nm. Further scaling causes excessive source-to-drain leakage and the loss of subthermionic switching in SG and DG devices with $L_{Ch} \leq 5$ nm and $L_{Ch} \leq 3$ nm, as highlighted in Figure 3 (g). Direct source-to-drain tunneling limits how steeply these devices can turn on. This tunneling is proportional to $\exp(-\sqrt{m_{\text{eff}}} \times l_t)$, where m_{eff} is the effective mass along the transport direction and l_t is the tunneling length. Hence, the rate of increase of the drain current when going from the OFF state to the ON state degrades with the reduction of the channel length of the device. We find that the rate of degradation is lower in DG devices compared to SG devices due to better elec-

trostatics in DG devices.

To counter the impact of increased source-to-drain tunneling, we increase the channel length of the double gate device with a gate length of 3 nm by adding ΔL_{SG} to $L_{SG/DG}$. The resulting device structure effectively increases the source-drain barrier width and height, thereby reducing the source-to-drain leakage and subthreshold leakage. However, there is a trade-off between ΔL_{SG} and ON-state performance due to reduced gate control over the extended channel^{49,50}. The simulated transport characteristics for various ΔL_{SG} values up to 3 nm [0, 0.5, 1.0, 1.5, 2.0, 3.0 nm] are shown in Figure S10 of the SI⁴⁴. We find that with increase in ΔL_{SG} , the source-to-drain leakage decreases. The device exhibits subthermionic behavior with a $SS_{\text{min}} < 30$ mV/decade, and $SS_{\text{avg}} < 37$ mV/decade over more than three decades of drain current at $\Delta L_{SG} \geq 2.0$ nm, with an ON-OFF ratio more than 10^3 , as shown in Figure 3 (h) and (i).

D. Edge Functionalization of MoSi₂N₄

Having demonstrated efficient subthreshold switching below 60 mV/decade in laterally confined MoSi₂N₄ devices with hydrogen passivation, a natural question to ask is what happens on passivating with other atoms^{51–54}. To address this, we subject 10-MoSi₂N₄ to different edge functionalization, by passivating the dangling bonds with H, F, and O, which are commonly used for edge termination^{51–57}. In exploring edge functionalization, we keep the coordination number of edge atoms to be the same as in the bulk 2D sample. We investigate several possible combinations of edge functionalization, which are listed in Table I.

Among all the edge functionalized MoSi₂N₄ nanoribbons mentioned above, two of the band structures are shown in Figure 4. In case of O-H-H terminated 10-MoSi₂N₄ shown in Figure 4 (a), E_G (~ 1.40 eV) is larger than the bandgap of 2H-H-H terminated 10-MoSi₂N₄. The two lowest energy conduction bands have a bandwidth of $E_{C,BW} \sim 0.27$ eV, and are separated from the next conduction band by ~ 0.33 eV. Our Bader charge analysis^{58,59} shows that the charge on each Mo atom is reduced by $0.31e$ in O-H-H terminated 10-MoSi₂N₄ compared to that in 2H-H-H terminated 10-MoSi₂N₄. As

Table I. Different edge functionalization schemes for MoSi₂N₄.

| S. No. | Edge Atoms Termination Scheme | Notation |
|--------|--|----------|
| 1 | (Mo, Si, N) \rightarrow (2H, H, H) | 2H-H-H |
| 2 | (Mo, Si, N) \rightarrow (2F, F, F) | 2F-F-F |
| 3 | (Mo, Si, N) \rightarrow (2F, H, H) | 2F-H-H |
| 4 | (Mo, Si, N) \rightarrow (2H, F, F) | 2H-F-F |
| 5 | (Mo, Si, N) \rightarrow (O, H, H) | O-H-H |
| 6 | (Mo, Si, N) \rightarrow (O, F, F) | O-F-F |
| 7 | (Mo-1, Mo-2, Si, N) \rightarrow (H, F, H, H) | HF-H-H |
| 8 | (Mo, Si, N) \rightarrow (N, H, H) | N-H-H |

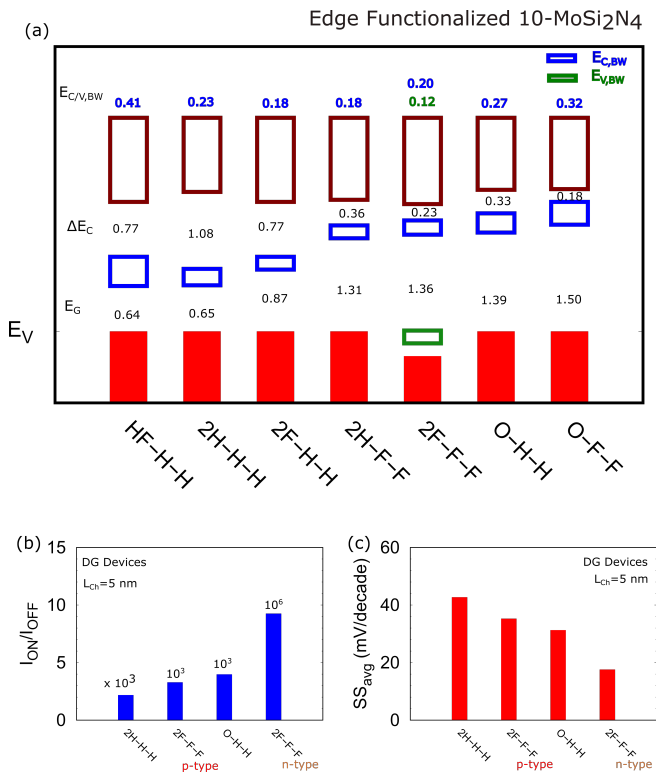


Figure 5. (a) Pictorial representation of the unique electronic properties of 10-MoSi₂N₄ with different terminations, such as HF-H-H, 2F-H-H, 2H-F-F, O-H-H, and O-F-F. All the studied structures have a narrow lowest energy conduction band which is separated from the higher-energy conduction band. 2F-F-F terminated 10-MoSi₂N₄ also has an isolated narrow valance band which can enable subthermionic switching in a p-type device. (b) Excellent ON/OFF ratio and (c) very low average subthreshold slope of DG devices based on 2H-H-H, O-H-H, and 2F-F-F terminated 10-MoSi₂N₄ as a channel material with $L_{Ch} = 5$ nm. While all of these offer extreme power efficiency in terms of transistor performance, the performance parameters for 2F-F-F terminated 10-MoSi₂N₄ are amongst the best reported values for any 2D material.

a result, the percentage contribution of the *d*-orbital of the edge Mo atoms is less (CBM 40% and VBM 15%) in O-H-H terminated 10-MoSi₂N₄, than that in 2H-H-H terminated 10-MoSi₂N₄ (CBM 67% and VBM 24%). For 2F-F-F terminated 10-MoSi₂N₄ [see Figure 4 (b)], the bandgap (~ 1.36 eV) is larger than the bandgap of purely 2H-H-H terminated 10-MoSi₂N₄. The two lowest energy conduction bands have a bandwidth of $E_{C,BW} \sim 0.20$ eV, and these are separated from the next conduction band by ~ 0.23 eV. Interestingly, we find that 2F-F-F terminated nanoribbon shows high energy filtering capability for holes also, having $E_{V,BW} \sim 0.12$ eV and separated from the nearest valance band by ~ 0.19 eV [see Figure 4 (b)]. Hence, it can be used to realize both n- and p-type steep-slope devices.

The most remarkable outcome of our detailed analysis of the electronic properties of edge functionalized

MoSi₂N₄ nanoribbon is its robust band structure, which has the same qualitative features irrespective of the choice of edge functionalization. Band diagrams of several possible combinations of edge functionalization are compared in Figure 5 (a), illustrating a wide range of values for E_G (0.64 eV - 1.50 eV) and ΔE_C (0.18 eV - 1.08 eV), while $E_{C,BW}$ value lies within a small range of 0.42 eV - 0.18 eV. The corresponding band structures are shown in Figure S5 of SI⁴⁴. Most of these structures have a narrow bandwidth conduction band which limits the long thermal tail of carriers and thermionic injection in the OFF state. This makes them suitable for low-power applications. Additionally, edge functionalization engineering offers a route to control their desired electronic properties. Amongst these, the 2F-F-F terminated nanoribbon is the only one having both narrow conduction and narrow valance bands. In addition, we find that the N-H-H terminated nanoribbon is metallic [see Figure S5 of SI⁴⁴]. In fact, such ‘cold’ metals can be used as a cold source contact in FETs, which is another way to achieve sub-60 mV/decade switching and overcome Boltzmann’s tyranny⁶⁰.

E. Transistors with functionalized MoSi₂N₄ and other materials in the series

The transfer characteristics of DG devices, with O-H-H terminated n-type, 2F-F-F terminated n-type, and 2F-F-F terminated p-type 10-MoSi₂N₄ as channel material is shown in Figure 4 (c-e). All the devices show subthermionic nature in drain current down to 5 nm channel length. More specifically, the drain current show subthermionic nature over more than five decades, eight decades, and three decades of drain current for devices with $L_{Ch} \leq 5$ nm based on n-type devices with O-H-H, and 2F-F-F termination, and p-type device with 2F-F-F termination, respectively.

The best performance of DG devices with $L_{Ch} = 5$ nm is shown in Figure 5 (b) and (c). All the devices show ON/OFF ratio of more than 10^3 and an average subthreshold slope of less than 45 mV/decade. However, the best performing device is n-type comprised of 2F-F-F terminated 10-MoSi₂N₄, owing to flat conduction band minima and hence low SDT leakage, with $I_{ON}/I_{OFF} > 10^6$ and $SS_{avg} < 20$ mV/decade. See Sec. E of the SI⁴⁴ for a more detailed analysis. The upper limit of devices’ performance is assessed as the ballistic nature of transport is considered. However, the presence of electron-phonon interaction could degrade the device’s performance, but the subthermionic nature of devices could be maintained^{61,62}.

Having demonstrated excellent low-power transistor characteristics for laterally confined and passivated MoSi₂N₄, we now explore other materials in the same series of compounds for ultra-low-power devices. Specifically, we extend the search in MA₂Z₄ the family, where M=Mo, Cr, Zr, Ti, Hf; A=Si, Ge; and Z=N, P, As. The calculated band diagrams for 2H-H-H terminated

10-MA₂Z₄ nanoribbon is shown in Figure 6. We find that there are several candidates in this family, having narrow bandwidth first valence or conduction bands, separated from nearby bands by a sizeable gap. This opens up the field for further exploration of MA₂Z₄ series of materials, for potential application in ultra-low power transistor applications as channel materials.

III. CONCLUSION

One of the major bottlenecks for making ultra-power-efficient transistors is decreasing the applied gate voltage for a 10-fold increase in the source-to-drain current during the conduction process. The bottleneck is controlled by the long thermal tail of the charge carriers, which leads to a large thermionic current in the OFF state. We propose a solution to this problem by using narrow bandwidth semiconductors as channel material. The narrow bandwidth of the conduction/valance band naturally restricts the long thermal tail of the charge carriers, reduces the thermionic current in the OFF state, and solves the problem of Boltzmann's tyranny.

We demonstrate this using the example of the laterally confined monolayer MoSi₂N₄. We show that passivated MoSi₂N₄ nano-ribbons have a narrow bandwidth conduction band, which is separated from nearby bands by a large bandgap. By combining first-principle calculations and nano-scale device simulations, we evaluate the performance of several transistors using differently terminated MoSi₂N₄ nano-ribbons as channel material. We find that devices with several differently terminated MoSi₂N₄ as channel material show a considerable performance improvement with a subthreshold slope much smaller than 60 mV/decade. Some of them can be used to realize both n- and p-type power-efficient transistors. We show that these unique electronic properties of narrow bandwidth are also shared by several other members of the MSi₂N₄ family of materials. Our work offers a new direction for engineering and exploring narrow bandwidth materials for enabling steep-slope transistors and ultra power-efficient computing.

Appendix A: Methods

1. Density Functional Theory Calculations

All the DFT-based first-principles calculations are performed using the projector augmented wave (PAW) potentials, as implemented in the Quantum ESPRESSO code suite^{63,64}. A Perdew-Burke-Ernzerhof (PBE)⁶⁵ based generalized gradient approximation (GGA) is used to include the exchange and correlation effects. The kinetic energy cut-off of the wave function and the charge density is set to 60 Ry and 600 Ry, respectively. The charge transfer is analyzed using the Bader partitioning scheme, in which the electron density is divided at zero flux surfaces^{58,59}. A 14 × 14 × 1 Monkhorst-Pack (MP)

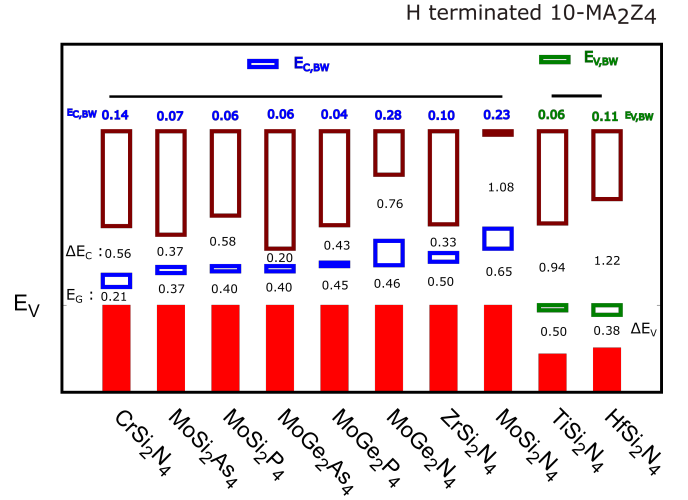


Figure 6. Pictorial representation of unique electronic properties different materials of the MA₂Z₄ series, with H termination. Going beyond MoSi₂N₄, several other materials in the same series also have similar bandstructure features as laterally confined MoSi₂N₄, which enable subthermionic switching for power efficient transistors.

k -mesh is used for Brillouin zone integration. For lateral confinement, a thick vacuum layer (~ 25 Å) is considered in y and z direction.

2. Device Simulations

The electronic band structure of the system is represented by a set of Wannier functions to upscale the system for device simulation via the Wannier90 code suite⁶⁶. The overlap matrix between the adjacent k points and the projection matrix is used as the input to calculate the Wannier functions. The resulting transformed Hamiltonian matrix in the basis of MLWFs is sparse in nature. We calculate the transmission coefficients $[T(E)]$ and potentials at each bias (V_{GS} , V_{DS}), by solving the Poisson and Schrödinger equations self-consistently in the NEGF formalism^{67,68}. The Landauer-Büttiker method is used to estimate the drain current, which can be expressed as

$$I_{DS} = \frac{2e}{h} \int_{-\infty}^{\infty} T(E, V_{GS}, V_{DS}) [f(E - \mu_S) - f(E - \mu_D)] dE.$$

Here, e is the elementary charge, h is the Planck constant and V_{GS} (V_{DS}) is the gate-source (drain-source) voltage. $T(E, V_{GS}, V_{DS})$ is the transmission coefficient at a given energy E and a bias (V_{GS}, V_{DS}). $\mu_{S/D}$ and $f(E - \mu_{S/D})$ are the fermi energy level and the Fermi-Dirac distribution function at source/drain, respectively. The tunneling probability, $T(E, V_{GS}, V_{DS})$ is calculated using

$$T(E, V_{GS}, V_{DS}) = \text{Trace}[\Gamma_S G^R \Gamma_D G^A]. \quad (\text{A1})$$

Here, $G^{R/A}$ is the retarded/advance Green functions, $\Gamma_{S/D}$ is the broadening from source/drain contacts and

E is the energy. Additionally, we have

$$\Gamma_{S/D}(E, V_{GS}, V_{DS}) = i[\Sigma_{S/D} - \Sigma_{S/D}^\dagger], \quad (\text{A2a})$$

$$G^R(E, V_{GS}, V_{DS}) = [EI - H - \Sigma]^{-1}, \quad (\text{A2b})$$

$$G^A(E, V_{GS}, V_{DS}) = [G^R(E, V_{GS}, V_{DS})]^\dagger. \quad (\text{A2c})$$

Here, I is the an identity matrix, $\Sigma_{S/D}$ is source/drain contact self-energy, $\Sigma = \Sigma_S + \Sigma_D$, and H is the Hamiltonian matrix representing the channel.

ACKNOWLEDGEMENTS

This work was supported in part by the Humboldt Foundation and in part by the Swarnajayanti Fellowship of the Department of Science and Technology (DST), Government of India under Grant DST/SJF/ETA-02/2017-18. The authors thank the CC-IITK for providing the HPC facility. We acknowledge the Science and Engineering Research Board (SERB, for projects MTR/2019/001520), and the Department of Science and Technology (DST, for project DST/NM/TUE/QM-6/2019(G)-IIT Kanpur) of the Government of India for financial support.

* keshari@iitk.ac.in

† bsomnath@iitk.ac.in

‡ chauhan@iitk.ac.in

§ amitag@iitk.ac.in

- 1 Adrian M. Ionescu and Heike Riel, "Tunnel field-effect transistors as energy-efficient electronic switches," *Nature* **479**, 329–337 (2011)
- 2 Qin Zhang, Wei Zhao, and A. Seabaugh, "Low-subthreshold-swing tunnel transistors," *IEEE Electron Device Letters* **27**, 297–300 (2006)
- 3 Venkatagirish Nagavarapu, Ritesh Jhaveri, and Jason C. S. Woo, "The tunnel source (pnpn) n-mosfet: A novel high performance transistor," *IEEE Transactions on Electron Devices* **55**, 1013–1019 (2008)
- 4 J. Appenzeller, Y.-M. Lin, J. Knoch, and Ph. Avouris, "Band-to-band tunneling in carbon nanotube field-effect transistors," *Phys. Rev. Lett.* **93**, 196805 (2004)
- 5 Sayeef Salahuddin and Supriyo Datta, "Use of negative capacitance to provide voltage amplification for low power nanoscale devices," *Nano Letters* **8**, 405–410 (2008)
- 6 Giovanni A. Salvatore, Didier Bouvet, and Adrian Mihai Ionescu, "Demonstration of subthreshold swing smaller than 60mv/decade in fe-fet with p(vdf-trfe)/sio2 gate stack," *2008 IEEE International Electron Devices Meeting*, 1–4 (2008)
- 7 Alexandru Rusu, Giovanni A. Salvatore, David Jiménez, and Adrian M. Ionescu, "Metal-ferroelectric-meta-oxide-semiconductor field effect transistor with sub-60mv/decade subthreshold swing and internal voltage amplification," in *2010 International Electron Devices Meeting* (2010) pp. 16.3.1–16.3.4
- 8 Mengwei Si, Chun-Jung Su, Chunsheng Jiang, Nathan J. Conrad, Hong Zhou, Kerry D. Maize, Gang Qiu, Chien-Ting Wu, Ali Shakouri, Muhammad A. Alam, and Peide D. Ye, "Steep-slope hysteresis-free negative capacitance mos2 transistors," *Nature Nanotechnology* **13**, 24–28 (2018)
- 9 M. H. Lee, P.-G. Chen, C. Liu, K.-Y. Chu, C.-C. Cheng, M.-J. Xie, S.-N. Liu, J.-W. Lee, S.-J. Huang, M.-H. Liao, M. Tang, K.-S. Li, and M.-C. Chen, "Prospects for ferroelectric hfxrox fets with experimentally cet=0.98nm, ssfor=42mv/dec, ssrev=28mv/dec, switch-off lt;0.2v, and hysteresis-free strategies," *2015 IEEE International Electron Devices Meeting (IEDM)*, 22.5.1–22.5.4 (2015)
- 10 Kai-Shin Li, Pin-Guang Chen, Tung-Yan Lai, Chang-Hsien Lin, Cheng-Chih Cheng, Chun-Chi Chen, Yun-Jie

- Wei, Yun-Fang Hou, Ming-Han Liao, Min-Hung Lee, Min-Cheng Chen, Jia-Min Sheih, Wen-Kuan Yeh, Fu-Liang Yang, Sayeef Salahuddin, and Chenming Hu, "Sub-60mv-swing negative-capacitance finfet without hysteresis," *2015 IEEE International Electron Devices Meeting (IEDM)*, 22.6.1–22.6.4 (2015)
- 11 Asif Islam Khan, Korok Chatterjee, Juan Pablo Duarte, Zhongyuan Lu, Angada Sachid, Sourabh Khandelwal, Ramamoorthy Ramesh, Chenming Hu, and Sayeef Salahuddin, "Negative capacitance in short-channel finfets externally connected to an epitaxial ferroelectric capacitor," *IEEE Electron Device Letters* **37**, 111–114 (2016)
- 12 B. Radisavljevic, A. Radenovic, J. Brivio, V. Giacometti, and A. Kis, "Single-layer mos2 transistors," *Nature Nanotechnology* **6**, 147–150 (2011)
- 13 Tania Roy, Mahmut Tosun, Jeong Seuk Kang, Angada B. Sachid, Sujay B. Desai, Mark Hettick, Chenming C. Hu, and Ali Javey, "Field-effect transistors built from all two-dimensional material components," *ACS Nano* **8**, 6259–6264 (2014)
- 14 Sujay B. Desai, Surabhi R. Madhvapathy, Angada B. Sachid, Juan Pablo Llinas, Qingxiao Wang, Geun Ho Ahn, Gregory Pitner, Moon J. Kim, Jeffrey Bokor, Chenming Hu, H.-S. Philip Wong, and Ali Javey, "Mos2 transistors with 1-nanometer gate lengths," *Science* **354**, 99–102 (2016)
- 15 Tianran Li, Teng Tu, Yuanwei Sun, Huixia Fu, Jia Yu, Lei Xing, Ziang Wang, Huimin Wang, Rundong Jia, Jinxiong Wu, Congwei Tan, Yan Liang, Yichi Zhang, Congcong Zhang, Yumin Dai, Chenguang Qiu, Ming Li, Ru Huang, Liying Jiao, Keji Lai, Binghai Yan, Peng Gao, and Hailin Peng, "A native oxide high- κ gate dielectric for two-dimensional electronics," *Nature Electronics* **3**, 473–478 (2020)
- 16 Fan Wu, He Tian, Yang Shen, Zhan Hou, Jie Ren, Guangyang Gou, Yabin Sun, Yi Yang, and Tian-Ling Ren, "Vertical mos2 transistors with sub-1-nm gate lengths," *Nature* **603**, 259–264 (2022)
- 17 Xiao Zou, Lu Liu, Jingping Xu, Hongjiu Wang, and Wing-Man Tang, "Few-layered mos2 field-effect transistors with a vertical channel of sub-10 nm," *ACS Applied Materials & Interfaces* **12**, 32943–32950 (2020)
- 18 Max C. Lemme, Deji Akinwande, Cedric Huyghebaert, and Christoph Stampfer, "2d materials for future heterogeneous electronics," *Nature Communications* **13**, 1392 (2022)

- ¹⁹ K. S. Novoselov, A. K. Geim, S. V. Morozov, D. Jiang, Y. Zhang, S. V. Dubonos, I. V. Grigorieva, and A. A. Firsov, “Electric field effect in atomically thin carbon films,” *American Association for the Advancement of Science* **306**, 666–669 (2004)
- ²⁰ Ganesh R. Bhimanapati, Zhong Lin, Vincent Meunier, Yeonwoong Jung, Judy Cha, Saptarshi Das, Di Xiao, Youngwoo Son, Michael S. Strano, Valentino R. Cooper, Liangbo Liang, Steven G. Louie, Emilie Ringe, Wu Zhou, Steve S. Kim, Rajesh R. Naik, Bobby G. Sumpter, Humberto Terrones, Fengnian Xia, Yeliang Wang, Jun Zhu, Deji Akinwande, Nasim Alem, Jon A. Schuller, Raymond E. Schaak, Mauricio Terrones, and Joshua A. Robinson, “Recent advances in two-dimensional materials beyond graphene,” *ACS Nano* **9**, 11509–11539 (2015)
- ²¹ Sheneve Z. Butler, Shawna M. Hollen, Linyou Cao, Yi Cui, Jay A. Gupta, Humberto R. Gutiérrez, Tony F. Heinz, Seung Sae Hong, Jiaying Huang, Ariel F. Ismach, Ezekiel Johnston-Halperin, Masaru Kuno, Vladimir V. Plashnitsa, Richard D. Robinson, Rodney S. Ruoff, Sayeef Salahuddin, Jie Shan, Li Shi, Michael G. Spencer, Mauricio Terrones, Wolfgang Windl, and Joshua E. Goldberger, “Progress, challenges, and opportunities in two-dimensional materials beyond graphene,” *ACS Nano* **7**, 2898–2926 (2013)
- ²² Yu-Chuan Lin, Bhakti Jariwala, Brian M. Bersch, Ke Xu, Yifan Nie, Baoming Wang, Sarah M. Eichfeld, Xiaotian Zhang, Tanushree H. Choudhury, Yi Pan, Rafik Addou, Christopher M. Smyth, Jun Li, Kehao Zhang, M. Aman Haque, Stefan Fölsch, Randall M. Feenstra, Robert M. Wallace, Kyeongjae Cho, Susan K. Fullerton-Shirey, Joan M. Redwing, and Joshua A. Robinson, “Realizing large-scale, electronic-grade two-dimensional semiconductors,” *ACS Nano* **12**, 965–975 (2018)
- ²³ Zhengyang Cai, Bilu Liu, Xiaolong Zou, and Hui-Ming Cheng, “Chemical vapor deposition growth and applications of two-dimensional materials and their heterostructures,” *Chemical Reviews* **118**, 6091–6133 (2018)
- ²⁴ Dumitru Dumcenco, Dmitry Ovchinnikov, Kolyo Marinov, Predrag Lazić, Marco Gibertini, Nicola Marzari, Oriol Lopez Sanchez, Yen-Cheng Kung, Daria Krasnozhan, Ming-Wei Chen, Simone Bertolazzi, Philippe Gillet, Anna Fontcuberta i Morral, Aleksandra Radenovic, and Andras Kis, “Large-area epitaxial monolayer mos₂,” *ACS Nano* **9**, 4611–4620 (2015)
- ²⁵ Achintya Priyadarshi, Yogesh Singh Chauhan, Somnath Bhowmick, and Amit Agarwal, “Large and anisotropic carrier mobility in monolayers of the ma₂z₄ series (m = cr, mo, w; a = si, ge; and z = n, p),” *Nanoscale* **14**, 11988–11997 (2022)
- ²⁶ Anan Bari Sarkar, Barun Ghosh, Bahadur Singh, Somnath Bhowmick, Hsin Lin, Arun Bansil, and Amit Agarwal, “k₂cos₂: A two-dimensional in-plane antiferromagnetic insulator,” *Phys. Rev. B* **102**, 035420 (2020)
- ²⁷ Barun Ghosh, Sougata Mardanya, Bahadur Singh, Xiaoting Zhou, Baokai Wang, Tay-Rong Chang, Chenliang Su, Hsin Lin, Amit Agarwal, and Arun Bansil, “Saddle-point van Hove singularity and dual topological state in pt₂hgse₃,” *Phys. Rev. B* **100**, 235101 (2019)
- ²⁸ Barun Ghosh, Shivam Puri, Amit Agarwal, and Somnath Bhowmick, “Snp₃: A previously unexplored two-dimensional material,” *The Journal of Physical Chemistry C* **122**, 18185–18191 (2018)
- ²⁹ Barun Ghosh, Bahadur Singh, R. Prasad, and Amit Agarwal, “Electric-field tunable dirac semimetal state in phos-
phorene thin films,” *Phys. Rev. B* **94**, 205426 (2016)
- ³⁰ Nicolò Oliva, Jonathan Backman, Luca Capua, Matteo Cavalieri, Mathieu Luisier, and Adrian M. Ionescu, “Wse₂/snse₂ vdw heterojunction tunnel fet with sub-thermionic characteristic and mosfet co-integrated on same wse₂ flake,” *npj 2D Materials and Applications* **4**, 5 (2020)
- ³¹ Chunsen Liu, Huawei Chen, Shuiyuan Wang, Qi Liu, Yungang Jiang, David Wei Zhang, Ming Liu, and Peng Zhou, “Two-dimensional materials for next-generation computing technologies,” *Nature Nanotechnology* **15**, 545–557 (2020)
- ³² Demetrio Logoteta, Marco G. Pala, Jean Choukroun, Philippe Dollfus, and Giuseppe Iannaccone, “A steep-slope MoS₂-nanoribbon mosfet based on an intrinsic cold-contact effect,” *IEEE Electron Device Letters* **40**, 1550–1553 (2019)
- ³³ Muhammad Nadeem, Iolanda Di Bernardo, Xiaolin Wang, Michael S. Fuhrer, and Dimitrie Culcer, “Overcoming boltzmann’s tyranny in a transistor via the topological quantum field effect,” *Nano Letters* **21**, 3155–3161 (2021)
- ³⁴ Chenguang Qiu, Fei Liu, Lin Xu, Bing Deng, Mengmeng Xiao, Jia Si, Li Lin, Zhiyong Zhang, Jian Wang, Hong Guo, *et al.*, “Dirac-source field-effect transistors as energy-efficient, high-performance electronic switches,” *Science* **361**, 387–392 (2018)
- ³⁵ Maomao Liu, Hemendra Nath Jaiswal, Simran Shahi, Sichen Wei, Yu Fu, Chaoran Chang, Anindita Chakravarty, Fei Yao, and Huamin Li, “Monolayer MoS₂ steep-slope transistors with record-high sub-60-mv/decade current density using dirac-source electron injection,” *IEEE International Electron Devices Meeting (IEDM)*, 12.5.1–12.5.4 (2020)
- ³⁶ Yi-Lun Hong, Zhibo Liu, Lei Wang, Tianya Zhou, Wei Ma, Chuan Xu, Shun Feng, Long Chen, Mao-Lin Chen, Dong-Ming Sun, Xing-Qiu Chen, Hui-Ming Cheng, and Wencai Ren, “Chemical vapor deposition of layered two-dimensional mosi₂n₄ materials,” *Science* **369**, 670–674 (2020)
- ³⁷ Liemao Cao, Guanghui Zhou, Qianqian Wang, L. K. Ang, and Yee Sin Ang, “Two-dimensional van der waals electrical contact to monolayer mosi₂n₄,” *Applied Physics Letters* **118**, 013106 (2021)
- ³⁸ A Bafekry, M Faraji, D M Hoat, M Shahrokhi, M M Fadlallah, F Shojaei, S A H Feghhi, M Ghergherehchi, and D Gogova, “MoSi₂n₄ single-layer: a novel two-dimensional material with outstanding mechanical, thermal, electronic and optical properties,” *Journal of Physics D: Applied Physics* **54**, 155303 (2021)
- ³⁹ Bohayra Mortazavi, Brahmanandam Javvaji, Fazel Shojaei, Timon Rabczuk, Alexander V. Shapeev, and Xiaoying Zhuang, “Exceptional piezoelectricity, high thermal conductivity and stiffness and promising photocatalysis in two-dimensional mosi₂n₄ family confirmed by first-principles,” *Nano Energy* **82**, 105716 (2021)
- ⁴⁰ Chao-chao Jian, Xiangchao Ma, Jianqi Zhang, and Xin Yong, “Strained mosi₂n₄ monolayers with excellent solar energy absorption and carrier transport properties,” *The Journal of Physical Chemistry C* **125**, 15185–15193 (2021)
- ⁴¹ Qianqian Wang, Liemao Cao, Shi-Jun Liang, Weikang Wu, Guangzhao Wang, Ching Hua Lee, Wee Liat Ong, Hui Ying Yang, Lay Kee Ang, Shengyuan A. Yang, and Yee Sin Ang, “Efficient ohmic contacts and built-in atomic sublayer protection in mosi₂n₄ and wsi₂n₄ monolayers,” *npj 2D Materials and Applications* **5**, 71 (2021)

- ⁴² Keshari Nandan, Barun Ghosh, Amit Agarwal, Somnath Bhowmick, and Yogesh S. Chauhan, “Two-dimensional mosi2n4: An excellent 2-d semiconductor for field-effect transistors,” *IEEE Transactions on Electron Devices*, 1–8 (2021)
- ⁴³ Jing Wang and M. Lundstrom, “Does source-to-drain tunneling limit the ultimate scaling of mosfets?” in *Digest. International Electron Devices Meeting*, (2002) pp. 707–710
- ⁴⁴ The Supporting information has more discussions on the i) structural and electronic properties of the MoA₂Z₄ series of materials, ii) their passivated structures, iii) and the transport properties of transistors with nanoribbon of MoSi₂N₄ with different passivations.
- ⁴⁵ Lei Wang, Yongpeng Shi, Mingfeng Liu, Yi-Lun Hong, Ming-Xing Chen, Ronghan Li, Qiang Gao, Wencai Ren, Hui-Ming Cheng, Yiyi Li, *et al.*, “Structure-driven intercalated architecture of septuple-atomic-layer *ma.2z.4* family with diverse properties from semiconductor to topological insulator to ising superconductor,” arXiv preprint arXiv:2008.02981 (2020)
- ⁴⁶ Rong Yang, Zhiwen Shi, Lianchang Zhang, Dongxia Shi, and Guangyu Zhang, “Observation of raman g-peak split for graphene nanoribbons with hydrogen-terminated zigzag edges,” *Nano Letters* **11**, 4083–4088 (2011)
- ⁴⁷ Xiaowei Zhang, Oleg V. Yazyev, Juanjuan Feng, Liming Xie, Chenggang Tao, Yen-Chia Chen, Liying Jiao, Zahra Pedramrazi, Alex Zettl, Steven G. Louie, Hongjie Dai, and Michael F. Crommie, “Experimentally engineering the edge termination of graphene nanoribbons,” *ACS Nano* **7**, 198–202 (2013)
- ⁴⁸ Yukinori Morita and Hiroshi Tokumoto, “Ideal hydrogen termination of si(001) surface by wet-chemical preparation,” *Applied Physics Letters* **67**, 2654–2656 (1995)
- ⁴⁹ A. Bansal, B.C. Paul, and K. Roy, “Modeling and optimization of fringe capacitance of nanoscale dgmos devices,” *IEEE Transactions on Electron Devices* **52**, 256–262 (2005)
- ⁵⁰ Keshari Nandan, Amit Agarwal, Somnath Bhowmick, and Yogesh S. Chauhan, “Performance investigation of p-FETs based on highly air-stable monolayer pentagonal PdSe₂,” *IEEE Transactions on Electron Devices*, 1–7 (2021)
- ⁵¹ Alejandro Lopez-Bezanilla, Jingsong Huang, Humberto Terrones, and Bobby G. Sumpter, “Structure and electronic properties of edge-functionalized armchair boron nitride nanoribbons,” *The Journal of Physical Chemistry C* **116**, 15675–15681 (2012)
- ⁵² Yi Ren, Fang Cheng, Z. H. Zhang, and Guanghui Zhou, “Half metal phase in the zigzag phosphorene nanoribbon,” *Scientific Reports* **8**, 2932 (2018)
- ⁵³ Xi Zhu and Haibin Su, “Excitons of edge and surface functionalized graphene nanoribbons,” *The Journal of Physical Chemistry C* **114**, 17257–17262 (2010)
- ⁵⁴ Alejandro Lopez-Bezanilla, Jingsong Huang, Humberto Terrones, and Bobby G. Sumpter, “Boron nitride nanoribbons become metallic,” *Nano Letters* **11**, 3267–3273 (2011)
- ⁵⁵ F. Cervantes-Sodi, G. Csányi, S. Piscanec, and A. C. Ferrari, “Edge-functionalized and substitutionally doped graphene nanoribbons: Electronic and spin properties,” *Phys. Rev. B* **77**, 165427 (2008)
- ⁵⁶ Liemao Cao, Xiaobo Li, Yun Li, and Guanghui Zhou, “Electrical properties and spintronic application of carbon phosphide nanoribbons with edge functionalization,” *J. Mater. Chem. C* **8**, 9313–9321 (2020)
- ⁵⁷ Mirco Panighel, Sabela Quiroga, Pedro Brandimarte, Cesar Moreno, Aran Garcia-Lekue, Manuel Vilas-Varela, Dulce Rey, Guillaume Sauthier, Gustavo Ceballos, Diego Peña, and Aitor Mugarza, “Stabilizing edge fluorination in graphene nanoribbons,” *ACS Nano* **14**, 11120–11129 (2020)
- ⁵⁸ Graeme Henkelman, Andri Arnaldsson, and Hannes Jónsson, “A fast and robust algorithm for bader decomposition of charge density,” *Computational Materials Science* **36**, 354–360 (2006)
- ⁵⁹ Min Yu and Dallas R. Trinkle, “Accurate and efficient algorithm for bader charge integration,” *The Journal of Chemical Physics* **134**, 064111 (2011)
- ⁶⁰ Fei Liu, “Switching at less than 60 mv/decade with a “cold” metal as the injection source,” *Phys. Rev. Applied* **13**, 064037 (2020)
- ⁶¹ D. Logoteta, J. Cao, M. Pala, P. Dollfus, Y. Lee, and G. Iannaccone, “Cold-source paradigm for steep-slope transistors based on van der waals heterojunctions,” *Phys. Rev. Research* **2**, 043286 (2020)
- ⁶² Demetrio Logoteta, Jiang Cao, Marco Pala, Paolo Marconcini, and Giuseppe Iannaccone, “Intrinsic sub-thermionic capabilities and high performance of easy-to-fabricate monolayer metal dihalide mosfets,” arXiv preprint arXiv:2106.12077 (2021)
- ⁶³ Paolo Giannozzi, Stefano Baroni, Nicola Bonini, Matteo Calandra, Roberto Car, Carlo Cavazzoni, Davide Ceresoli, Guido L Chiarotti, Matteo Cococcioni, Ismaila Dabo, Andrea Dal Corso, Stefano de Gironcoli, Stefano Fabris, Guido Fratesi, Ralph Gebauer, Uwe Gerstmann, Christos Gougoussis, Anton Kokalj, Michele Lazzeri, Layla Martin-Samos, Nicola Marzari, Francesco Mauri, Riccardo Mazzarello, Stefano Paolini, Alfredo Pasquarello, Lorenzo Paulatto, Carlo Sbraccia, Sandro Scandolo, Gabriele Sclauzero, Ari P Seitsonen, Alexander Smogunov, Paolo Umari, and Renata M Wentzcovitch, “QUANTUM ESPRESSO: a modular and open-source software project for quantum simulations of materials,” *Journal of Physics: Condensed Matter* **21**, 395502 (2009)
- ⁶⁴ P Giannozzi, O Andreussi, T Brumme, O Bunau, M Buongiorno Nardelli, M Calandra, R Car, C Cavazzoni, D Ceresoli, M Cococcioni, N Colonna, I Carnimeo, A Dal Corso, S de Gironcoli, P Delugas, R A DiStasio, A Ferretti, A Floris, G Fratesi, G Fugallo, R Gebauer, U Gerstmann, F Giustino, T Gorni, J Jia, M Kawamura, H-Y Ko, A Kokalj, E Küçükbenli, M Lazzeri, M Marsili, N Marzari, F Mauri, N L Nguyen, H-V Nguyen, A Otero de-la Roza, L Paulatto, S Poncé, D Rocca, R Sabatini, B Santra, M Schlipf, A P Seitsonen, A Smogunov, I Timrov, T Thonhauser, P Umari, N Vast, X Wu, and S Baroni, “Advanced capabilities for materials modelling with quantum ESPRESSO,” *Journal of Physics: Condensed Matter* **29**, 465901 (2017)
- ⁶⁵ John P. Perdew, Kieron Burke, and Matthias Ernzerhof, “Generalized gradient approximation made simple,” *Phys. Rev. Lett.* **77**, 3865–3868 (1996)
- ⁶⁶ Arash A. Mostofi, Jonathan R. Yates, Giovanni Pizzi, Young-Su Lee, Ivo Souza, David Vanderbilt, and Nicola Marzari, “An updated version of wannier90: A tool for obtaining maximally-localised wannier functions,” *Computer Physics Communications* **185**, 2309 – 2310 (2014)
- ⁶⁷ Supriyo Datta, *Quantum transport: atom to transistor* (Cambridge university press, 2005)

- ⁶⁸ S. Bruzzone, G. Iannaccone, N. Marzari, and G. Fiori, “An open-source multiscale framework for the simulation of nanoscale devices,” [IEEE Transactions on Electron Devices](#) **61**, 48–53 (2014)